



1 **Open fires in Greenland: an unusual event and its impact**
2 **on the albedo of the Greenland Ice Sheet**

3

4 **Nikolaos Evangeliou^{1,*}, Arve Kylling¹, Sabine Eckhardt¹, Viktor Myroniuk²,**
5 **Kerstin Stebel¹, Ronan Paugam³, Sergiy Zibtsev², Andreas Stohl¹**

6

7 ¹Norwegian Institute for Air Research (NILU), Department of Atmospheric and Climate
8 Research (ATMOS), Kjeller, Norway.

9 ²National University of Life and Environmental Sciences of Ukraine, Kiev, Ukraine.

10 ³King's College London, London, United Kingdom.

11

12 * Corresponding author: N. Evangeliou (Nikolaos.Evangeliou@nilu.no)

13



14 **Abstract**

15 Highly unusual open fires burned in Western Greenland between 31 July and 21 August
16 2017, after a period of warm, dry and sunny weather. The fires burned on peat lands that
17 became vulnerable to fires by permafrost thawing. We used several satellite data sets to
18 estimate that the total area burned was about 2345 hectares. Based on assumptions of typical
19 burn depths and BC emission factors for peat fires, we estimate that the fires consumed a fuel
20 amount of about 117 kt C and produced BC emissions of about 23.5 t. We used the
21 Lagrangian particle dispersion model to simulate the atmospheric BC transport and
22 deposition. We find that the smoke plumes were often pushed towards the Greenland Ice
23 Sheet by westerly winds and thus a large fraction of the BC emissions (7 t or 30%) was
24 deposited on snow or ice covered surfaces. The calculated BC deposition was small compared
25 to BC deposition from global sources, but not entirely negligible. Analysis of aerosol optical
26 depth data from three sites in Western Greenland in August 2017 showed strong influence of
27 forest fire plumes from Canada, but little impact of the Greenland fires. Nevertheless,
28 CALIOP lidar data showed that our model captured very effectively the presence and
29 structure of the plume from the Greenland fires. The albedo changes and instantaneous
30 surface radiative forcing in Greenland due to the fire BC emissions were estimated with the
31 SNICAR model and the uvspec model from the libRadtran radiative transfer software
32 package. We estimate that the maximum albedo change due to the BC deposition was about
33 0.006, too small to be measured by satellites or other means. The average instantaneous
34 surface radiative forcing over Greenland at noon on 31 August was 0.03 W m^{-2} , with locally
35 occurring maximum values of 0.63 W m^{-2} . The average value is at least an order of magnitude
36 smaller than the radiative forcing due to BC from other sources. Overall, the fires burning in
37 Greenland in summer of 2017 had little impact on BC deposition on the Greenland Ice Sheet,
38 causing almost negligible extra radiative forcing. This was due to the – in a global context –
39 still rather small size of the fires. However, the very large fraction of the BC emissions
40 deposited on the Greenland Ice Sheet makes these fires very efficient climate forcers on a per
41 unit emission basis. If the expected further warming of Greenland produces much larger fires
42 in the future, this could indeed cause substantial albedo changes and thus lead to accelerated
43 melting of the Greenland Ice Sheet. The fires burning in 2017 may be a harbinger of such
44 future changes.

45



46 **1 Introduction**

47 In August 2017 public media reported unprecedented fire events in Western Greenland
48 (BBC News, 2017; New Scientist Magazine, 2017). These events were documented with
49 airborne photographs (SERMITSIAQ, 2017) and satellite images (NASA, 2017b) and raised
50 public concerns about the effects of climate change and possible impacts of soot emissions on
51 ice melting. Historically, wildfires have occurred infrequently on Greenland, because three-
52 quarters of the island is covered by a permanent ice sheet and permafrost is found on most of
53 the ice-free land (Abdalati and Steffen, 2001). Permafrost, or permanently frozen soil, lies
54 under a several meters thick “active” soil layer that thaws seasonally. But in certain areas,
55 where the permafrost layer starts melting, it can expose peat, a material consisting of only
56 partially decomposed vegetation that forms in wetlands over the course of hundreds of years
57 or longer. Peatlands, also known as bogs and moors, are the earliest stage in the formation of
58 coal. Globally, the amount of carbon stored in peats exceeds that stored in vegetation and is
59 similar in size to the current atmospheric carbon pool (Turetsky et al., 2014). When peatlands
60 dry, they are often affected by fires burning into the peat layers. Peat fires are difficult to
61 extinguish and they often burn until all the organic matter is consumed. Smoldering peat fires
62 already are the largest fires on Earth in terms of their carbon footprint (Turetsky et al., 2014).
63 For Greenland, it has been suggested that degradation of peat will accelerate towards 2080
64 (Daanen et al., 2011) and that the area affected by the fires in August 2017 is particularly
65 vulnerable to permafrost thawing (Daanen et al., 2011).

66 Fires in the high northern latitudes release significant amounts of CO₂, CH₄, N₂O and
67 black carbon (BC), and their emissions are often transported into Arctic regions (Cofer III et
68 al., 1991; Hao et al., 2016a; Hao and Ward, 1993; Shi et al., 2015). BC is the most strongly
69 light-absorbing component of the atmospheric aerosol (Bond et al., 2013) and is formed by
70 the incomplete combustion of fossil fuels, biofuels, and biomass. It is important due to its
71 human health (Lelieveld et al., 2015) and climate impacts (Sand et al., 2015), and its
72 atmospheric lifetime of 3–11 days (Bond et al., 2013) facilitates transport over long distances
73 (Forster et al., 2001; Stohl et al., 2006). BC from mid-latitude sources can thus reach remote
74 areas such as the Arctic. BC absorbs solar radiation in the atmosphere and has a significant
75 impact on cloud formation. It also decreases surface albedo when deposited on ice and snow
76 and can accelerate melting processes (Hansen and Nazarenko, 2004). This raises particular
77 concerns about the effect of fires burning in the immediate vicinity of the Greenland Ice
78 Sheet. If a large fraction of the BC emitted by such fires is deposited on the ice, these fires



79 may be extremely effective in further enhancing the already accelerating melting of the
80 Greenland Ice Sheet (AMAP, 2017). BC emissions from such high latitude fires may also
81 have a substantial effect on the albedo of sea ice.

82 Here we study transport and deposition of BC over the Greenland Ice Sheet from the
83 fires that occurred in Western Greenland in August 2017, which probably represent the largest
84 fires that have occurred on Greenland in modern times. Since the fires occurred in an area
85 entirely lacking ground-based observations, we use satellite data and a Lagrangian
86 atmospheric dispersion model for our study.

87 **2 Methods**

88 **2.1 Definition of burned area**

89 Remote sensing has been useful for delineating fire perimeters, characterizing burn
90 severity and planning post-fire restoration activities in different regions. The use of satellite
91 imaging is particularly important for fire monitoring in remote areas of the Arctic due to
92 difficult ground access. Coordinates of fire locations (hot spots) were downloaded from
93 FIRMS (Fire Information for Resource Management System) (NASA, 2017a). For the
94 mapping of the burned area, Sentinel 2A images were used. To delineate fire perimeters and
95 define burn severity precisely, we used Landsat 8 Operational Land Imager (OLI) together
96 with Sentinel 1A and Sentinel 2A images (see Table 1) by applying the differenced
97 Normalized Burn Ratio (dNBR) (Key and Benson, 2006):

$$98 \quad dNBR = NBR_{pre-fire} - NBR_{post-fire} \quad (\text{Eq. 1})$$

99 Normalized burn ratios for pre- ($NBR_{pre-fire}$) and postfire ($NBR_{post-fire}$) images from
100 Sentinel 2A can be calculated using radiances for near- and shortwave infrared bands (bands 8
101 (NIR) and 12 (SWIR2) at 0.835 μm and 2.202 μm , respectively):

$$102 \quad NBR = \frac{1000 \cdot (NIR - SWIR2)}{NIR + SWIR2} \quad (\text{Eq. 2})$$

103 The methodology of applying a dNBR index to assess the impact of fires has been used in
104 forests of the Northern and Western USA (French et al., 2008; Key and Benson, 2006) and
105 elsewhere (Escuin et al., 2008; Sunderman and Weisberg, 2011).

106 The burned severity mosaics were created using Sentinel 2A images corrected for
107 atmospheric scattering (see Chavez, 1988). Pre- and post-fire images were used to create
108 cloudless mosaics for the area where the Greenland fires burned. A Maximum Value



109 Composite (MVC) procedure (Holben, 1986) was used to select pixels from each band that
110 were not cloud covered and have a high value of Normalized Difference Vegetation Index
111 (NDVI). Additional classification rules were imposed to map burn severity more precisely,
112 due to the sensitivity of NBR to changes in vegetation and soil moisture. Manually delineated
113 fire perimeters were applied and all areas outside were classified as unburned. We have used
114 common dNBR severity levels (Key and Benson, 2006) that are presented in Figure 1. The
115 occasionally dense cloud cover was the main obstacle in reconstructing fire dynamics. As an
116 independent source of information, active fires from MODIS satellite product MCD14DL
117 (Giglio et al., 2003) are plotted in Supplemental Information (SI) Figure S 1. These confirm
118 our results.

119 **2.2 Injection altitudes, assumptions on biomass consumption and emissions** 120 **factors**

121 Injection heights into the atmosphere of the emitted smoke were simulated with version
122 2 of the Plume Rise Model (PRM) (Paugam et al., 2015) which is implemented in the Global
123 Fire Assimilation System (GFAS) emission inventory (Rémy et al., 2017). The model
124 (hereafter referred to as PRMv2) is a further development of PRM (Freitas et al., 2006, 2010)
125 and has already been used in previous studies of fire events (Evangelidou et al., 2015, 2016).
126 The model simulates a profile of smoke detrainment for every single fire, from which two
127 metrics are extracted: (i) a detrainment layer (i.e. where the detrainment rate is > 50% of its
128 global maximum) and (ii) an injection height (InjH, the top of the detrainment layer). Instead
129 of using the GFAS product, which uses the same statistics as in the PRMv2 InjH calculation,
130 we ran the model for every detected fire assuming a 6 h persistence and using the same
131 conversion factor as Kaiser et al. (2012) to estimate the biomass consumption. PRMv2 mass
132 detrainment profiles are then time integrated and extracted at $1^\circ \times 1^\circ$ spatial resolution with a
133 500 m vertical mesh to estimate the 3D distribution of biomass burned. Figure S 2 (SI) shows
134 for all fires recorded in the MODIS fire product (Justice et al., 2002) during the fire period
135 (31 July – 21 August 2017) the horizontal distribution of the median height of the emitted
136 biomass and its integration over the longitude (right panel). Fires in Greenland showed a
137 maximum injection height of around 2 km, but according to PRMv2 the majority of the
138 emissions (90%) remained below 800 m. Low injection heights mostly inside the daytime
139 planetary boundary layer are quite typical for smoldering fires including peat fires (Ferguson
140 et al., 2003) such as those burning in Greenland (see below). For modeling the dispersion of



141 BC released from the Greenland fires, the emission profiles from PRMv2 were ingested into
142 the Lagrangian particle dispersion model FLEXPART (see section 2.3).

143 Wildfires in boreal peatlands in the Canadian Arctic and in Alaska typically have
144 (shallow) burn depths of 1–10 cm and consume 20–30 t C ha⁻¹ (Benscoter and Wieder, 2003;
145 Shetler et al., 2008), which is often re-sequestered in 60–140 years after the fire (Turetsky et
146 al., 2011; Wieder et al., 2009). Given that fire return intervals can be as short as 100–150
147 years in sub-humid continental peatlands (Wieder et al., 2009), and may exceed 2000 years in
148 humid climates (Lavoie and Pellerin, 2007), northern peatlands are generally resilient to
149 wildfire (Magnan et al., 2012). For example, in peatlands of Northern Russia, organic matter
150 available for combustion has been estimated to be 121.8 t C ha⁻¹ for forested lands and 21.3 t
151 C ha⁻¹ for non-forested lands (Smirnov et al., 2015). Accordingly, a severe wildfire that
152 burned within an afforested peatland in the Scottish Highlands during the summer of 2006
153 had a mean depth of burn of 17.5±2.0 cm (range: 1–54 cm) and a carbon loss of 96±15 t C ha⁻¹
154 (Davies et al., 2013). In contrast, tropical peatlands can have deep burn depths of 40–50 cm
155 and release an average of 300–450 t C ha⁻¹ (Page et al., 2015; Reddy et al., 2015). In the
156 present study, we assume an average amount of organic fuel available for combustion for the
157 Greenland peat fires of August 2017 of 100 t C ha⁻¹, guided by values suggested elsewhere
158 (Smirnov et al., 2015).

159 The emissions of BC from peat fires in Greenland were calculated using the following
160 formula (Seiler and Crutzen, 1980; Urbanski et al., 2011):

$$161 \quad E_{BC} = A \times FL \times \alpha \times EF \quad \text{Eq. 1}$$

162 where E_{BC} is the BC emission from the fire (kg); A is the burned area (ha); FL is the mass of
163 the fuel available for combustion (kg C ha⁻¹); α is the dimensionless combustion
164 completeness, which was adopted from Hao et al. (2016) for litter and duff fuels (50%) and
165 EF is the emission factor of BC (kg kg⁻¹) that was adopted from Akagi et al. (2011) for
166 peatland fires (0.0002 kg kg⁻¹). Fuel consumption is calculated as the product of burned area,
167 fuel loading and combustion completeness ($A \times FL \times \alpha$).

168 **2.3 Atmospheric modeling**

169 The emissions of BC obtained from Eq. 1 were fed to the Lagrangian particle dispersion
170 model FLEXPART version 10.2 (Stohl et al., 2005) to simulate BC transport and deposition.
171 This model was originally developed for calculating the dispersion of radioactive material
172 from nuclear emergencies, but since then it has been used for many other applications (e.g.,



173 Fang et al., 2014; Stohl et al., 2011, 2013). The model has a detailed description of particle
174 dispersion in the boundary layer and a convection scheme to simulate particle transport in
175 clouds (Forster et al., 2007). The model was driven by hourly $0.5^{\circ} \times 0.5^{\circ}$ operational analyses
176 from the European Centre for Medium-Range Weather Forecasts (ECMWF). Concentration
177 and deposition fields were recorded in a global domain of $1^{\circ} \times 1^{\circ}$ spatial resolution with three
178 hourly outputs. To capture the spatiotemporal variability of BC over the Greenland Ice Sheet,
179 a nested domain with $0.05^{\circ} \times 0.05^{\circ}$ resolution was used. The simulations accounted for wet
180 and dry deposition, assuming a particle density of 2000 kg m^{-3} and a logarithmic size
181 distribution with an aerodynamic mean diameter of $0.4 \mu\text{m}$ and a standard deviation of 0.3.
182 The wet deposition scheme considers below-cloud and in-cloud scavenging separately based
183 on cloud liquid water and cloud ice content, precipitation rate and cloud depth from ECMWF,
184 as described in Grythe et al. (2017).

185 To compare BC concentrations in Greenland due to the emissions of the Greenland fires
186 to those due to BC emissions occurring elsewhere, we used the so-called “retroplume” mode
187 of FLEXPART. In this mode, computational particles from a receptor region were tracked 30
188 days back in time. We used four receptor regions: Northwestern (-62°E to -42°E , 72°N to
189 83°N), Southwestern (-62°E to -42°E , 61°N to 72°N), Northeastern (-42°E to -17°E , 72°N to
190 83°N) and Southeastern Greenland (-42°E to -17°E , 61°N to 72°N). The retroplume mode
191 allowed identification of the origin of BC through calculated footprint emission sensitivities
192 (often also called source-receptor relationships) that express the sensitivity of the BC surface
193 concentration at the receptor to emissions on the model output grid. If these emissions are
194 known, the BC concentrations at the receptor can be calculated as the product of the emission
195 flux and the emission sensitivity. Also, detailed source contribution maps can be calculated,
196 showing which regions contributed to the simulated concentration. For the anthropogenic
197 emissions, we used the ECLIPSE (Evaluating the CLimate and Air Quality ImPacts of
198 ShortlivEd Pollutants) version 5 (Klimont et al., 2017) emission data set. For the biomass
199 burning emissions outside Greenland, we used global MODIS-satellite hot spot data (Giglio et
200 al., 2003) and a simple emission scheme (Stohl et al., 2007), with emission factors for BC
201 adopted from Andreae and Merlet (2001) and Akagi et al. (2011).

202 **2.4 Radiative forcing calculations**

203 The radiative forcing (RF) of the emitted BC was calculated using the uvspec model
204 from the libRadtran radiative transfer software package (Emde et al., 2016; Mayer and
205 Kylling, 2005). Liquid water and ice water clouds were adopted from ECMWF operational



206 analysis data. No aerosols except those emitted from the Greenland fires were included. As
207 such, the RF calculations represent a maximum estimate of the effect of BC from the
208 Greenland fires. For snow-covered surfaces, deposited BC was assumed to reside in the
209 uppermost 5 mm. Below 5 mm the snow was assumed to be without any impurities. The
210 albedo of the snow was calculated with the SNICAR model in a two-layer configuration
211 (Flanner et al., 2007, 2009).

212 RF was calculated at the top and bottom of the atmosphere at $1^\circ \times 1^\circ$ resolution. The
213 radiative transfer equation was solved in the independent pixel approximation using the
214 DISORT model in pseudo-spherical geometry with improved treatment of peaked phase
215 functions (Buras et al., 2011; Dahlback and Stamnes, 1991; Stamnes et al., 1988). Radiation
216 absorption by gases was taken from the Kato et al. (1999) parameterization modified as
217 described in the libRadtran documentation and Wandji Nyamsi et al. (2015).

218 **2.5 Remote sensing of the smoke plume**

219 To confirm the presence of BC from fires in Greenland and elsewhere in the atmosphere
220 over Greenland, we used the AERONET (AErosol RObotic NETwork) data (Holben et al.,
221 1998). AERONET provides globally distributed observations of spectral aerosol optical depth
222 (AOD), inversion products, and precipitable water in diverse aerosol regimes. We chose data
223 from three stations that were close to the 2017 fires and for which cloud-free data exist for
224 most of the simulated period, namely Kangerlussuaq (50.62°W – 66.99°N), Narsarsuaq
225 (45.52°W – 61.16°N) and Thule (68.77°W – 76.51°N). Their locations are shown in Figure S 1.
226 We display Level 1.5 (cloud-screened) AOD data at 500 nm from the AERONET version 3
227 direct-sun spectral deconvolution algorithm (SDA version 4.1) product (download
228 15/11/2017) for the simulated period (31 July to 31 August 2017).

229 To examine in particular the vertical depth of the smoke, we used data from the
230 CALIOP (Cloud-Aerosol Lidar with Orthogonal Polarization) lidar on the CALIPSO (Cloud-
231 Aerosol Lidar and Infrared Pathfinder Satellite Observations) platform (Winker et al., 2009).
232 CALIOP provides profiles of backscatter at 532 nm and 1064 nm, as well as the degree of the
233 linear polarization of the 532 nm signal. For altitudes below 8.3 km lidar profiles at 532 nm
234 are available with a vertical resolution of 30 m. We have utilized the level 1 data products
235 (version 3.40) of total attenuated backscatter at 532 nm. This signal responds to aerosols (like
236 BC) as well as water and ice clouds, which in most cases can be distinguished based on their



237 differences in optical properties. The data were downloaded via ftp from the ICARE Data and
238 Services Center (<http://www.icare.univ-lille1.fr/>).

239 **3 Results**

240 **3.1 Indications of early permafrost degradation and fuel availability**

241 Table 1 reports burned areas in August 2017 over Greenland from GlobCover 2009
242 (Global Land Cover Map at 300 m resolution) (Arino et al., 2008). In total, 2345 hectares
243 burned between 31 July and 21 August 2017 (Figure 1). We estimate that about 117 kt of
244 carbon were consumed by these fires. The area burned is not large compared to the global
245 area burned each year of 464 million hectares, or the areas burned in boreal North America
246 (2.6 million hectares) or boreal Asia (9.8 million hectares) (Randerson et al., 2012), but still
247 highly unusual for Greenland.

248 It is not yet known how these fires started. Fires on carbon-rich soils can be initiated by
249 an external source, e.g. lightning, flaming wildfire and firebrand, or self-heating. The fires
250 burned relatively close to the town of Sisimut, so it is quite possible that humans started the
251 fires. Self-heating is another possibility as porous solid fuels can undergo spontaneous
252 exothermic reactions in oxidative atmospheres at low temperatures (Drysdale, 2011;
253 Restuccia et al., 2017b). This process starts by slow exothermic oxidation at ambient
254 temperature, causing a temperature increase, which is determined by the imbalance between
255 the rate of heat generation and the rate of heat losses (Drysdale, 2011). Fire initiated by self-
256 heating ignition is a well-known hazard for many natural materials (Fernandez Anez et al.,
257 2015; Restuccia et al., 2017a; Wu et al., 2015) and can also occur in natural soils (Restuccia
258 et al., 2017b). Southwestern Greenland was under anticyclonic influence during the last week
259 of July and according to the MODIS ESDIS worldview tool, direct sunshine occurred for
260 eight consecutive days before the fires started at the end of July 2017. It might be possible
261 that this long period of almost continuous insolation at these latitudes in July heated the soil
262 enough to self-ignite. In any case, the continuous sunshine had dried the soil, making it
263 susceptible to fire.

264 The fact that these fires were burning for about three weeks but spread relatively slowly
265 compared to above-ground vegetation fires indicates that the main fuel was probably peat.
266 The predominant vegetation in Western Greenland varies from carbon-rich *Salix glauca* low
267 shrubs (mean canopy height: 95 cm), mainly at low altitude south-facing slopes with deep



268 soils and ample moisture, to dwarf-shrubs and thermophilous graminoid vegetation (Arctic
269 steppe) at higher altitudes (Jedrzejek et al., 2013). In addition, the observed smoke was nearly
270 white, indicating damp fuel, such as freshly thawed permafrost, which produces smoke rich in
271 organic carbon (OC) aerosol (Stockwell et al., 2016). Notice that while OC is not strongly
272 absorbing, it may contain some absorbing brown carbon, which would add to the albedo
273 reduction of snow by BC. On the other hand, BC emission factors are relatively low for peat
274 fires (see Akagi et al., 2011).

275 Literally no fires should be expected in Greenland, since there is little available fuel as
276 it has been suggested by global models and validated by observations (Daanen et al., 2011;
277 Stendel et al., 2008); the only way to provide substantial amounts of fuel in Greenland is
278 permafrost degradation. However, it has been suggested that significant permafrost loss in
279 Greenland may occur only by the end of the 21st century (Daanen et al., 2011; Stendel et al.,
280 2008). The fires in 2017 might indicate that significant permafrost degradation has occurred
281 sooner than expected.

282 **3.2 Transport and deposition of BC in Greenland**

283 We estimate that about 23.5 t of BC were released from the Greenland fires in August
284 2017 (Table 1). According to the FLEXPART model simulations, these emissions were
285 transported and deposited following the prevailing atmospheric circulation as shown in Figure
286 2. Due to the low injection altitude of the releases within the boundary layer, transport was
287 relatively slow and thus most BC initially remained quite close to its emission source. Slow
288 transport was also favored by mostly anticyclonic influence during the first half of August. It
289 seems that even though katabatic winds from the Greenland Ice Sheet occasionally
290 transported the plume westwards, most of the time the large-scale circulation pushed the
291 plume back towards Greenland. Consequently, a large fraction of the emitted BC was
292 deposited in Southwestern Greenland. On 3 August a small portion of the emitted BC was
293 lifted higher into the atmosphere and was transported to the east and deposited in the middle
294 of the Ice Sheet over the course of the following two days (4 and 5 August). From 5 to 8
295 August, when the fires were particularly intense, BC was transported to the south, where most
296 of it was deposited at the southern part of the Ice Sheet and close to the coastline. At the same
297 time, another branch of the plume was moving to the north depositing BC over Greenland's
298 western coastline up to 80°N, while around 10 August the plume circulated north- and then
299 eastwards on the northwestern sector of the anti-cyclone and BC was deposited to the
300 northern part of the Ice Sheet until 13 August. From around 16 August, a cyclone approached



301 from the northwest and the smoke was briefly transported directly eastwards along the
302 southern edge of the cyclone. Strong rain associated with the cyclone's frontal system appears
303 to have largely extinguished the fire by 17 or 18 August, although smaller patches may have
304 continued smoldering for a few more days before they also died out. The exact fire behavior
305 after 16 August is difficult to determine because of frequent dense cloud cover. However,
306 satellite imagery on 21 August shows no smoke anymore in the area where the fires had
307 burned.

308 The total deposition of BC from the fires in Greenland is shown in Figure 2b. About 9 t
309 of BC from the Greenland fires in summer 2017 were deposited over Greenland, which is
310 about 39% of the fires' total emissions. About 7 t (30% of the total emissions) were deposited
311 on snow or ice covered surfaces. Most of the rest was deposited in the Baffin Bay between
312 Greenland and Canada and in the Atlantic Ocean.

313 With 30% of the emissions deposited on snow or ice surfaces, Greenland fires may have
314 a relatively large efficiency for causing albedo changes on the Greenland Ice Sheet. By
315 comparison, the respective BC deposition on snow and ice surfaces over Greenland from
316 global emissions of BC was only 0.4% (39 kt) of the emissions. Even the total deposition of
317 BC in the Arctic ($>67^{\circ}\text{N}$) was only about 3% (215 kt). This indicates the high relative
318 potential of Greenland fires to pollute the cryosphere (on a per unit emission basis), giving
319 them a particularly high radiative forcing efficiency. Considering that the projected rise of
320 Greenland temperatures is expected to result in further degradation of the permafrost (Daanen
321 et al., 2011) and, hence, likely resulting in more and larger peat fires on Greenland, this
322 constitutes a potentially important climate feedback which could accelerate melting of the
323 glaciers and ice sheet of Greenland and enhance Arctic warming.

324 We also calculated the concentration of the deposited BC in Greenland snow (Figure 3)
325 by taking the ratio of deposited BC and the amount of water deposited by rain or snow fall
326 during the same time period (31 July to 31 August 2017). As expected, BC snow
327 concentrations show the same general patterns as the simulated deposition of BC with the
328 highest concentrations obtained close to the source. High BC in snow concentrations were
329 also computed in some regions of the Ice Sheet due to relatively intense precipitation events.
330 By contrast, dry deposition of BC over the Ice Sheets was low (Figure 3). Dry deposition was
331 responsible for a major fraction of the deposition only in regions where the plume was
332 transported during dry weather, and in most of these regions total deposition was low. A
333 notable exception is the region close to the fires, where dry deposition was relatively



334 important due to the generally dry weather when the fires were burning. The average
335 calculated concentration of BC on the Ice Sheet was estimated to be $<1 \text{ ng g}^{-1}$, but in some
336 areas snow concentrations reached up to 3 ng g^{-1} . These higher values are substantial
337 considering that measured concentrations of BC in snow typically range up to 16 ng g^{-1} in
338 most of Greenland (Doherty et al., 2010).

339 3.3 Impact from other emissions in Northern Hemisphere

340 In summertime 2017, intense wildfires were reported in British Columbia, Western
341 Canada (NASA, 2017c), and fires also burned at mid latitudes in Eurasia, as is typical during
342 spring and summer (Hao et al., 2016b). Previous studies of wildfires have shown that the
343 produced energy can be sufficient to loft smoke above the boundary layer by supercell
344 convection (Fromm et al., 2005) even up to stratospheric altitudes (Leung et al., 2007). As a
345 result, BC can become subject to long-range transport over long distances (Forster et al.,
346 2001; Stohl et al., 2007). To examine the impact of these fires in Greenland, average footprint
347 emission sensitivities were calculated for four compartments of Greenland (Northwestern,
348 Southwestern, Northeastern and Southeastern Greenland) for the period 31 July to 31 August
349 2017 and the results are shown in Figure S 3 together with the active fires in the Northern
350 Hemisphere from 10 July to 31 August 2017 adopted from the MODIS satellite product
351 (MCD14DL) (Giglio et al., 2003). As shown in Figure S 3, fires in Alaska might have
352 affected BC concentrations in Greenland, as the corresponding emission sensitivities are the
353 highest in North America. On the contrary, BC emitted from fires in Eurasia seems to have
354 affected Greenland less.

355 Using gridded emissions for BC, the contribution of both biomass burning and
356 anthropogenic sources to surface BC concentrations in the four different regions over
357 Greenland (Northwestern, Northeastern, Southwestern and Southeastern Greenland, Figure 4)
358 was calculated (see section 2.3). Fires affected the northern part of Greenland more than the
359 southern part with an average concentration of about 30 ng m^{-3} , almost twice the respective
360 average for Southern Greenland ($\approx 16 \text{ ng m}^{-3}$). About one third of the BC originated from
361 wildfires in Eurasia and the rest from North America where the year 2017 appears to have
362 been a particularly high fire year. The anthropogenic contribution to surface BC over
363 Greenland was only about 14% to 50% of the total contribution from all biomass burning
364 sources (Figure 4), similar to what has been suggested previously for the Arctic in summer
365 (Winiger et al., 2017). In contrast to biomass burning, the anthropogenic contribution is larger
366 in Southern Greenland due to the shorter distance from the main emission areas of North



367 America and Western Europe. The BC concentrations that are calculated here for the studied
368 fire period (31 July to 31 August 2017) are relatively high compared to those reported
369 previously. For instance, von Schneidemesser et al. (2009) observed an annual average BC
370 concentration of 20 ng m^{-3} at Summit (Greenland) in 2006, while Massling et al. (2015)
371 reported a summer average BC concentration of 11 ng m^{-3} at station Nord (Greenland)
372 between May 2011 and August 2013. We attribute this to more active fires during the study
373 period than in other years.

374 To compare how important Northern Hemispheric biomass burning emissions were for
375 the air over Greenland, we present time-series of surface BC concentrations in Northwestern,
376 Northeastern, Southwestern and Southeastern Greenland from the fires in Greenland and from
377 all the other wildfire emissions occurring outside Greenland (North Hemisphere) for the same
378 period of time (Figure S 4). The calculated dosages for the same time period were also
379 computed. The fires in Greenland affected mainly its western part with concentrations that
380 reached up to 4.8 ng m^{-3} (Southwestern Greenland on 10 August) and 4.4 ng m^{-3}
381 (Northwestern Greenland on 12 August), while BC concentrations in the eastern part
382 remained significantly lower (Figure S 4). These concentrations are substantial considering
383 that the observed surface BC concentrations in Greenland in summer are usually below 20 ng m^{-3}
384 (ng m^{-3}) (Massling et al., 2015). Surface BC due to wildfires occurring outside Greenland was also
385 low most of the time in the studied period (up to 10 ng m^{-3} at maximum) except for a large
386 peak between 19 and 23 August that mainly affected Northern Greenland (Figure S 4). The
387 concentrations during this episodic peak were as high as 27 ng m^{-3} . During the same period,
388 the contribution from anthropogenic emissions was also a few ng m^{-3} (Figure S 4). BC
389 dosages for the simulation period (31 July – 10 August 2017) in Western Greenland due to the
390 Greenland fires were about one order of magnitude smaller than dosages from fires elsewhere
391 but of the same order of magnitude as BC originating from anthropogenic emissions.

392 4 Discussion

393 4.1 A validation attempt

394 There are few observations available that can be used for validating our model results.
395 We use the AERONET and CALIOP data for some qualitative comparisons. Contours of
396 simulated vertical distribution of BC and column-integrated simulated BC from fires inside
397 and outside Greenland are plotted together with time-series of measured AOD at a
398 wavelength of 500 nm for the AERONET stations Kangerlussuaq, Narsarsuaq and Thule



399 (Figure 5). It can be seen that observed AOD variations were in very good agreement with the
400 variation of simulated column-integrated BC from fires outside Greenland (mainly in
401 Canada), confirming that the transport of these fire plumes was well captured by FLEXPART.
402 Good examples are the peaks at Kangerlussuaq on 24 August, at Narsarsuaq on 19 August
403 and at Thule on 21 August (Figure 5) that are attributed to the Canadian fires. The simulated
404 contribution of the Greenland fires to simulated BC burdens was negligible by comparison,
405 except at Kangerlussuaq in the beginning of August when the Greenland fire emissions were
406 the highest. This station is less than 100 km away from where the fires burned, but not in the
407 main direction of the BC plume transport. It seems the period of simulated fire influence
408 corresponds to a small increase of the observed AOD values of up to 20% (Figure 5).

409 To validate the smoke plume's vertical extent, we used the CALIOP data. These data
410 were only available from 5 August 2017 onward and frequent dense cloud cover inhibited
411 lidar observations in the altitudes below the clouds. High aerosol backscatter was only found
412 in the close vicinity of the fires. Figure 6a shows NASA's ESDIS view of the plume on 14
413 August 2017 at 6 UTC (available: [https://worldview.earthdata.nasa.gov/?p=geographic&l=MODIS_Aqua_CorrectedReflectance_TrueColor\(hidden\),MODIS_Terra_CorrectedReflectance_TrueColor,MODIS_Fires_Terra,MODIS_Fires_Aqua,Reference_Labels\(hidden\),Reference_Features,Coastlines&t=2017-08-14&z=3&v=-54.13349998138993,66.35888052399868,-50.32103113049877,69.08420005412792](https://worldview.earthdata.nasa.gov/?p=geographic&l=MODIS_Aqua_CorrectedReflectance_TrueColor(hidden),MODIS_Terra_CorrectedReflectance_TrueColor,MODIS_Fires_Terra,MODIS_Fires_Aqua,Reference_Labels(hidden),Reference_Features,Coastlines&t=2017-08-14&z=3&v=-54.13349998138993,66.35888052399868,-50.32103113049877,69.08420005412792)), where
414 a clear smoke signal was recorded. The structure of the plume can be identified in the
415 CALIOP curtain by its increased attenuated backscatter below ~1.5 km above sea level (black
416 line denotes the orography of the area) between 52°E and 51°E (white line in Figure 6b).
417 Another cloud of enhanced attenuated backscatter is evident at 4–5 km altitude between
418 50.5°E and 48.5°E. This mid-tropospheric plume was not studied but is likely due to aerosol
419 transport from the North American fires. These large wildfires are eager to lift smoke at
420 stratospheric altitudes as a result of super-cell convection and they have already shown to be
421 present as such altitudes in Greenland during the study period (see Figure 5). As shown in
422 Figure 6c (red line), the CALIOP overpass transects directly the simulated plume of the
423 Greenland fires. Notice that the simulated plume also agrees very well with the smoke as seen
424 in NASA's ESDIS picture (Figure 6a). The vertical distribution of simulated BC as a function
425 of longitude is illustrated in Figure 6d. It corresponds very well to the vertical distribution of
426 aerosols observed by CALIOP (Figure 6b). In particular, the smoke resides at altitudes below
427 1.5 km and at exactly the same location both in the simulations and observations.
428
429
430
431



432 **4.2 Effect on snow and ice surfaces**

433 The instantaneous radiative forcing (IRF) at the bottom of the atmosphere (BOA) for
434 noon on 31 August 2017 is depicted in Figure 7. This day is shown because almost all BC
435 emitted by the fires had been deposited before, thus giving a high IRF via albedo reduction
436 due to BC contamination of snow. Cloudless conditions were assumed in Figure 7a, while in
437 Figure 7b water and ice water clouds were adopted from ECMWF. For the cloudless
438 conditions, the IRF is largest around the fire site and at locations with relatively large BC
439 deposits. The maximum IRF is 1.82 W m^{-2} , while the average for Greenland is 0.05 W m^{-2} .
440 For the IRF including clouds the maximum BOA RF is 0.63 W m^{-2} , and the average 0.03 W m^{-2} .
441 For IRF at the top of the atmosphere (TOA), the corresponding values are 0.59 W m^{-2} and
442 0.03 W m^{-2} . Figure 7c depicts the temporal behaviour of the TOA IRF averaged over
443 Greenland (red line). In addition the daily averaged IRF is shown (green line). The blue line
444 in Figure 7b shows the value for the pixel with maximum IRF. The daily averaged IRF is
445 seen to increase as the plume from the fires spreads out and starts to decline after the fires
446 were extinguished at the end of the month. The fact that the reduction towards end of August
447 is relatively slow is caused by the effect of the albedo reduction, which persists until clean
448 snow covers the polluted snow. According to Hansen et al. (2005) the TOA IRF of BC
449 approximates the adjusted RF as reported by Myhre et al. (2013). In Table 8.4, Myhre et al.
450 (2013) estimated the global averaged RF due to BC between 1750 and 2011 to be $+0.40$
451 $(+0.05 \text{ to } +0.80) \text{ W m}^{-2}$. For Greenland, Skeie et al. (2011) calculated the RF to be less than
452 about 0.2 W m^{-2} due to BC originating from fossil fuel and biofuel combustion relative to
453 preindustrial times (1750). Thus, the calculated RF due to the Greenland fires for cloudy
454 conditions is about one order of magnitude smaller compared with the RF due to BC from all
455 global anthropogenic sources.

456 The albedo reduction at 550 nm due to the deposited BC is shown in Figure 7c. The
457 maximum albedo change is about 0.006. This albedo change has an impact on the radiative
458 forcing, but it is too small to be measured by satellites. For example, MODIS albedo
459 estimates have been compared to in situ albedo measurements in Greenland by Stroeve et al.
460 (2005). They found that the root mean square error between MODIS and in situ albedo values
461 was ± 0.04 for high quality flagged MODIS albedo retrievals. Unmanned Aerial Vehicle
462 (UAV) measurements over Greenland made by Burkhart et al. (2017) have uncertainties of
463 similar magnitude. The albedo changes due to BC from the fires are generally an order of
464 magnitude smaller (Figure 7c) and thus too small to be detected by present UAV and satellite
465 instruments and retrieval methods (Warren, 2013).



466 **5 Conclusions**

467 The conclusions from our study of the unusual open fires burning in Greenland between
468 31 July and 21 August 2017 are the following:

- 469 • The fires burned on peat lands that became vulnerable by permafrost thawing. The region
470 where the fires burned was identified previously as being susceptible to permafrost
471 melting; however, large-scale melting was expected to occur only towards the end of the
472 21st century. The 2017 fires show that at least in some locations substantial permafrost
473 thawing is occurring already now.
- 474 • The total area burned was about 2345 hectares. We estimate that the fires consumed a fuel
475 amount of about 117 kt C and produced BC emissions of about 23.5 t.
- 476 • The Greenland fires were small compared to fires burning at the same time in North
477 America and Eurasia, but a large fraction of their BC emissions (30% or 7 t) was
478 deposited on the Greenland Ice Sheet or glaciers. This BC deposition was small compared
479 to BC deposition from global anthropogenic and biomass burning sources, but not entirely
480 negligible.
- 481 • Measurements of aerosol optical depth at three sites in Western Greenland in August 2017
482 were strongly influenced by forest fires in Canada burning at the same time, but the
483 Greenland fires had an observable impact at the closest station.
- 484 • A comparison of the simulated BC releases in FLEXPART with the vertical cross-section
485 of total attenuation backscatter (at 532 nm) from CALIOP lidar showed that the
486 spatiotemporal evolution and particularly the top height of the plume was captured by the
487 model.
- 488 • We estimate that the maximum albedo change due to the BC deposition was about 0.006,
489 too small to be measured by satellites or other means. The average instantaneous surface
490 radiative forcing over Greenland at noon on 31 August was 0.03 W m^{-2} , with locally
491 occurring maximum values of 0.63 W m^{-2} . The average value is at least an order of
492 magnitude smaller than the radiative forcing due to BC from other sources.
- 493 • We conclude that the fires burning in Greenland in summer of 2017 had little impact on
494 BC deposition on the Greenland Ice Sheet, causing almost negligible extra radiative
495 forcing. This was due to the – in a global context - still rather small size of the fires.
496 However, the very large fraction of the BC emissions deposited on the Greenland Ice
497 Sheet makes these fires very efficient climate forcers on a per unit emission basis. If the
498 expected further warming of Greenland produces much larger fires in the future, this could



499 indeed cause substantial albedo changes and thus lead to accelerated melting of the
500 Greenland Ice Sheet.

501

502 *Data availability.* All data used for the present publication can be obtained from the
503 corresponding author upon request.

504

505 *Competing financial interests.* The authors declare no competing financial interests.

506

507 *Acknowledgements.* This study was partly supported by the Arctic Monitoring and
508 Assessment Programme (AMAP) and was conducted as part of the Nordic Centre of
509 Excellence eSTICC (Nordforsk 57001). We acknowledge the use of imagery from the NASA
510 Worldview application (<https://worldview.earthdata.nasa.gov/>) operated by the
511 NASA/Goddard Space Flight Center Earth Science Data and Information System (ESDIS)
512 project. We thank Brent_Holben and local site managers for their effort in establishing and
513 maintaining the AERONET sites used in this investigation. We thank NASA/CNES engineers
514 and scientists for making CALIOP data available. The lidar data were downloaded from the
515 ICARE Data and Service Center.

516

517 *Author contributions.* NE performed the simulations, analyses, wrote and coordinated the
518 paper. AK performed the radiation calculations and wrote parts of the paper. VM and SZ
519 performed GIS analysis for the burned area calculations. RP made all the runs for the
520 injection height calculations using the PRMv2 model. KS analysed satellite data for AOD and
521 CALIOP, SE and AS commented and coordinated the manuscript. All authors contributed to
522 the final version of the manuscript.

523

524 **References**

- 525 Abdalati, W. and Steffen, K.: Greenland Ice Sheet melt extent:1979-1999, J. Geophys. Res.
526 Atmos., 106(D24), 33983–33988, doi:10.1029/2001JD900181, 2001.
- 527 Akagi, S. K., Yokelson, R. J., Wiedinmyer, C., Alvarado, M. J., Reid, J. S., Karl, T., Crounse, J.
528 D. and Wennberg, P. O.: Emission factors for open and domestic biomass burning for use
529 in atmospheric models, Atmos. Chem. Phys., 11(9), 4039–4072, doi:10.5194/acp-11-
530 4039-2011, 2011.
- 531 AMAP: Snow, Water, Ice and Permafrost. Summary for Policy-makers, Arctic Monitoring
532 and Assessment Programme (AMAP), Oslo, Norway. [online] Available from:
533 [https://www.amap.no/documents/doc/Snow-Water-Ice-and-Permafrost.-Summary-
534 for-Policy-makers/1532](https://www.amap.no/documents/doc/Snow-Water-Ice-and-Permafrost.-Summary-for-Policy-makers/1532) (Accessed 27 November 2017), 2017.
- 535 Andreae, M. O. and Merlet, P.: Emissions of trace gases and aerosols from biomass
536 burning, Global Biogeochem. Cycles, 15(4), 955–966, doi:10.1029/2000GB001382,



- 537 2001.
- 538 Arino, O., Bicheron, P., Achard, F., Latham, J., Witt, R. and Weber, J.-L.: Globcover: The
539 most detailed protrait of Earth, Eur. Sp. Agency Bull., 136(November), 24–31,
540 doi:WOS:000261325400004, 2008.
- 541 BBC News: “Unusual” Greenland wildfires linked to peat, [online] Available from:
542 <http://www.bbc.com/news/science-environment-40877099> (Accessed 6 September
543 2017), 2017.
- 544 Benscoter, B. W. and Wieder, R. K.: Variability in organic matter lost by combustion in a
545 boreal bog during the 2001 Chisholm fire, Can. J. For. Res., 33(12), 2509–2513,
546 doi:10.1139/x03-162, 2003.
- 547 Bond, T. C., Doherty, S. J., Fahey, D. W., Forster, P. M., Berntsen, T., Deangelo, B. J., Flanner,
548 M. G., Ghan, S., Kärcher, B., Koch, D., Kinne, S., Kondo, Y., Quinn, P. K., Sarofim, M. C.,
549 Schultz, M. G., Schulz, M., Venkataraman, C., Zhang, H., Zhang, S., Bellouin, N., Guttikunda,
550 S. K., Hopke, P. K., Jacobson, M. Z., Kaiser, J. W., Klimont, Z., Lohmann, U., Schwarz, J. P.,
551 Shindell, D., Storelvmo, T., Warren, S. G. and Zender, C. S.: Bounding the role of black
552 carbon in the climate system: A scientific assessment, J. Geophys. Res. Atmos., 118(11),
553 5380–5552, doi:10.1002/jgrd.50171, 2013.
- 554 Buras, R., Dowling, T. and Emde, C.: New secondary-scattering correction in DISORT with
555 increased efficiency for forward scattering, J. Quant. Spectrosc. Radiat. Transf., 112(12),
556 2028–2034, doi:10.1016/j.jqsrt.2011.03.019, 2011.
- 557 Chavez, P. S.: An improved dark-object subtraction technique for atmospheric scattering
558 correction of multispectral data, Remote Sens. Environ., 24(3), 459–479,
559 doi:10.1016/0034-4257(88)90019-3, 1988.
- 560 Cofer III, W. R., Levine, J. S., Winstead, E. L. and Stocks, B. J.: New estimates of nitrous
561 oxide emissions from biomass burning, Nature, 349(6311), 689–691 [online] Available
562 from: <http://dx.doi.org/10.1038/349689a0>, 1991.
- 563 Daanen, R. P., Ingeman-Nielsen, T., Marchenko, S. S., Romanovsky, V. E., Foged, N.,
564 Stendel, M., Christensen, J. H. and Hornbech Svendsen, K.: Permafrost degradation risk
565 zone assessment using simulation models, Cryosphere, 5(4), 1043–1056,
566 doi:10.5194/tc-5-1043-2011, 2011.
- 567 Dahlback, A. and Stamnes, K.: A new spherical model for computing the radiation field
568 available for photolysis and heating at twilight, Planet. Space Sci., 39(5), 671–683,
569 doi:10.1016/0032-0633(91)90061-E, 1991.
- 570 Davies, G. M., Gray, A., Rein, G. and Legg, C. J.: Peat consumption and carbon loss due to
571 smouldering wildfire in a temperate peatland, For. Ecol. Manage., 308, 169–177,
572 doi:10.1016/j.foreco.2013.07.051, 2013.
- 573 Doherty, S. J., Warren, S. G., Grenfell, T. C., Clarke, A. D. and Brandt, R. E.: Light-absorbing
574 impurities in Arctic snow, Atmos. Chem. Phys., 10(23), 11647–11680, doi:10.5194/acp-
575 10-11647-2010, 2010.
- 576 Drysdale, D.: An Introduction to Fire Dynamics, 3rd Editio., John Wiley & Sons, Ltd.,
577 2011.
- 578 Emde, C., Buras-Schnell, R., Kylling, A., Mayer, B., Gasteiger, J., Hamann, U., Kylling, J.,
579 Richter, B., Pause, C., Dowling, T. and Bugliaro, L.: The libRadtran software package for
580 radiative transfer calculations (version 2.0.1), Geosci. Model Dev., 9(5), 1647–1672,
581 doi:10.5194/gmd-9-1647-2016, 2016.
- 582 Escuin, S., Navarro, R. and Fernández, P.: Fire severity assessment by using NBR
583 (Normalized Burn Ratio) and NDVI (Normalized Difference Vegetation Index) derived
584 from LANDSAT TM/ETM images, Int. J. Remote Sens., 29(4), 1053–1073,
585 doi:10.1080/01431160701281072, 2008.



- 586 Evangeliou, N., Balkanski, Y., Cozic, A., Hao, W. M., Mouillot, F., Thonicke, K., Paugam, R.,
587 Zibtsev, S., Mousseau, T. A., Wang, R., Poulter, B., Petkov, A., Yue, C., Cadule, P., Koffi, B.,
588 Kaiser, J. W., Møller, A. P. and Classen, A. T.: Fire evolution in the radioactive forests of
589 Ukraine and Belarus: Future risks for the population and the environment, *Ecol.*
590 *Monogr.*, 85(1), 49–72, doi:10.1890/14-1227.1, 2015.
- 591 Evangeliou, N., Zibtsev, S., Myroniuk, V., Zhurba, M., Hamburger, T., Stohl, A., Balkanski,
592 Y., Paugam, R., Mousseau, T. A., Møller, A. P. and Kireev, S. I.: Resuspension and
593 atmospheric transport of radionuclides due to wildfires near the Chernobyl Nuclear
594 Power Plant in 2015: An impact assessment, *Sci. Rep.*, 6, 26062 [online] Available from:
595 <http://www.nature.com/srep/2016/160517/srep26062/full/srep26062.html>, 2016.
- 596 Fang, X., Thompson, R. L., Saito, T., Yokouchi, Y., Kim, J., Li, S., Kim, K. R., Park, S., Graziosi,
597 F. and Stohl, A.: Sulfur hexafluoride (SF₆) emissions in East Asia determined by inverse
598 modeling, *Atmos. Chem. Phys.*, 14(9), 4779–4791, doi:10.5194/acp-14-4779-2014,
599 2014.
- 600 Faulkner Burkhart, J., Kylling, A., Schaaf, C. B., Wang, Z., Bogren, W., Storvold, R., Solbø, S.,
601 Pedersen, C. A. and Gerland, S.: Unmanned aerial system nadir reflectance and MODIS
602 nadir BRDF-adjusted surface reflectances intercompared over Greenland, Cryosphere,
603 11(4), 1575–1589, doi:10.5194/tc-11-1575-2017, 2017.
- 604 Ferguson, S. A., Collins, R. L., Ruthford, J. and Fukuda, M.: Vertical distribution of
605 nighttime smoke following a wildland biomass fire in boreal Alaska, *J. Geophys. Res.*,
606 108(June), D23, 4743, doi:10.1029/2002JD003324, doi:10.1029/2002JD003324, 2003.
- 607 Fernandez Anez, N., Garcia Torrent, J., Medic Pejic, L. and Grima Olmedo, C.: Detection of
608 incipient self-ignition process in solid fuels through gas emissions methodology, *J. Loss*
609 *Prev. Process Ind.*, 36, 343–351, doi:10.1016/j.jlp.2015.02.010, 2015.
- 610 Flanner, M. G., Zender, C. S., Randerson, J. T. and Rasch, P. J.: Present-day climate forcing
611 and response from black carbon in snow, *J. Geophys. Res. Atmos.*, 112(11), 1–17,
612 doi:10.1029/2006JD008003, 2007.
- 613 Flanner, M. G., Zender, C. S., Hess, P. G., Mahowald, N. M., Painter, T. H., Ramanathan, V.
614 and Rasch, P. J.: Springtime warming and reduced snow cover from carbonaceous
615 particles, *Atmos. Chem. Phys.*, 9, 2481–2497, doi:10.5194/acp-9-2481-2009, 2009.
- 616 Forster, C., Wandering, U., Wotawa, G., James, P., Mattis, I., Althausen, D., Simmonds, P.,
617 O'Doherty, S., Jennings, S. G., Kleefeld, C., Schneider, J., Trickl, T., Kreipl, S., Jäger, H. and
618 Stohl, A.: Transport of boreal forest fire emissions from Canada to Europe, *J. Geophys.*
619 *Res.*, 106, 22887, doi:10.1029/2001JD900115, 2001.
- 620 Forster, C., Stohl, A. and Seibert, P.: Parameterization of convective transport in a
621 Lagrangian particle dispersion model and its evaluation, *J. Appl. Meteorol. Climatol.*,
622 46(4), 403–422, doi:10.1175/JAM2470.1, 2007.
- 623 Freitas, S. R., Longo, K. M., Chatfield, R., Latham, D., Silva Dias, M. a. F., Andreae, M. O.,
624 Prins, E., Santos, J. C., Gielow, R. and Carvalho, J. a.: Including the sub-grid scale plume
625 rise of vegetation fires in low resolution atmospheric transport models, *Atmos. Chem.*
626 *Phys. Discuss.*, 6(6), 11521–11559, doi:10.5194/acpd-6-11521-2006, 2006.
- 627 Freitas, S. R., Longo, K. M., Trentmann, J. and Latham, D.: Technical Note: Sensitivity of 1-
628 D smoke plume rise models to the inclusion of environmental wind drag, *Atmos. Chem.*
629 *Phys.*, 10(2), 585–594, doi:10.5194/acp-10-585-2010, 2010.
- 630 French, N., Kasischke, E., Hall, R., Murphy, K., Verbyla, D., Hoy, E. and Allen, J.: Using
631 Landsat data to assess fire and burn severity in the North American boreal forest region:
632 an overview and summary of results, *Int. J. Wildl. Fire*, 17(4), 443–462,
633 doi:10.1071/WF08007, 2008.
- 634 Fromm, M., Bevilacqua, R., Servranckx, R., Rosen, J., Thayer, J. P., Herman, J. and Larko, D.:



- 635 Pyro-cumulonimbus injection of smoke to the stratosphere: Observations and impact of
636 a super blowup in northwestern Canada on 3-4 August 1998, *J. Geophys. Res. D Atmos.*,
637 110(8), 1–17, doi:10.1029/2004JD005350, 2005.
- 638 Giglio, L., Descloitres, J., Justice, C. O. and Kaufman, Y. J.: An enhanced contextual fire
639 detection algorithm for MODIS, *Remote Sens. Environ.*, 87(2–3), 273–282,
640 doi:10.1016/S0034-4257(03)00184-6, 2003.
- 641 Grythe, H., Kristiansen, N. I., Groot Zwaaftink, C. D., Eckhardt, S., Ström, J., Tunved, P.,
642 Krejci, R. and Stohl, A.: A new aerosol wet removal scheme for the Lagrangian particle
643 model FLEXPARTv10, *Geosci. Model Dev.*, 10, 1447–1466, doi:10.5194/gmd-10-1447-
644 2017, 2017.
- 645 Hansen, J. and Nazarenko, L.: Soot climate forcing via snow and ice albedos, *Proc. Natl.*
646 *Acad. Sci. U. S. A.*, 101(2), 423–428, doi:10.1073/pnas.2237157100, 2004.
- 647 Hansen, J., Sato, M., Ruedy, R., Nazarenko, L., Lacis, A., Schmidt, G. A., Russell, G., Aleinov,
648 I., Bauer, M., Bauer, S., Bell, N., Cairns, B., Canuto, V., Chandler, M., Cheng, Y., Del Genio, A.,
649 Faluvegi, G., Fleming, E., Friend, A., Hall, T., Jackman, C., Kelley, M., Kiang, N., Koch, D.,
650 Lean, J., Lerner, J., Lo, K., Menon, S., Miller, R., Minnis, P., Novakov, T., Oinas, V., Perlwitz,
651 J., Perlwitz, J., Rind, D., Romanou, A., Shindell, D., Stone, P., Sun, S., Tausnev, N., Thresher,
652 D., Wielicki, B., Wong, T., Yao, M. and Zhang, S.: Efficacy of climate forcings, *J. Geophys.*
653 *Res. D Atmos.*, 110(18), 1–45, doi:10.1029/2005JD005776, 2005.
- 654 Hao, W. M. and Ward, D. E.: Methane production from global biomass burning, *J.*
655 *Geophys. Res. Atmos.*, 98(D11), 20657–20661, doi:10.1029/93JD01908, 1993.
- 656 Hao, W. M., Petkov, A., Nordgren, B. L., Silverstein, R. P., Corley, R. E., Urbanski, S. P.,
657 Evangeliou, N., Balkanski, Y. and Kinder, B.: Daily black carbon emissions from fires in
658 Northern Eurasia from 2002 to 2013, *Geosci. Model Dev. Discuss.*, (April), 1–24,
659 doi:10.5194/gmd-2016-89, 2016a.
- 660 Hao, W. M., Petkov, A., Nordgren, B. L., Silverstein, R. P., Corley, R. E., Urbanski, S. P.,
661 Evangeliou, N., Balkanski, Y. and Kinder, B.: Daily black carbon emissions from fires in
662 Northern Eurasia from 2002 to 2013, *Geosci. Model Dev.*, 9, 4461–4474,
663 doi:10.5194/gmd-9-4461-2016, 2016b.
- 664 Holben, B. N.: Characteristics of maximum-value composite images from temporal
665 AVHRR data, *Int. J. Remote Sens.*, 7(11), 1417–1434, doi:10.1080/01431168608948945,
666 1986.
- 667 Holben, B. N., Eck, T. F., Slutsker, I., Tanré, D., Buis, J. P., Setzer, A., Vermote, E., Reagan, J.
668 A., Kaufman, Y. J., Nakajima, T., Lavenu, F., Jankowiak, I. and Smirnov, A.: AERONET—A
669 Federated Instrument Network and Data Archive for Aerosol Characterization, *Remote*
670 *Sens. Environ.*, 66(1), 1–16, doi:10.1016/S0034-4257(98)00031-5, 1998.
- 671 Jedrzejek, B., Drees, B., Daniëls, F. J. A. and Hölzel, N.: Vegetation pattern of mountains in
672 West Greenland - a baseline for long-term surveillance of global warming impacts, *Plant*
673 *Ecol. Divers.*, 6(3–4), 405–422, doi:10.1080/17550874.2013.802049, 2013.
- 674 Justice, C. O., Giglio, L., Korontzi, S., Owens, J., Morisette, J. T., Roy, D., Descloitres, J.,
675 Alleaume, S., Petitcolin, F. and Kaufman, Y.: The MODIS fire products, *Remote Sens.*
676 *Environ.*, 83(1–2), 244–262, doi:10.1016/S0034-4257(02)00076-7, 2002.
- 677 Kaiser, J. W., Heil, A., Andreae, M. O., Benedetti, A., Chubarova, N., Jones, L., Morcrette, J. J.,
678 Razinger, M., Schultz, M. G., Suttie, M. and Van Der Werf, G. R.: Biomass burning
679 emissions estimated with a global fire assimilation system based on observed fire
680 radiative power, *Biogeosciences*, 9(1), 527–554, doi:10.5194/bg-9-527-2012, 2012.
- 681 Kato, S., Ackerman, T. P., Mather, J. H. and Clothiaux, E. E.: The k-distribution method and
682 correlated-k approximation for a shortwave radiative transfer model, *J. Quant.*
683 *Spectrosc. Radiat. Transf.*, 62(1), 109–121, doi:10.1016/S0022-4073(98)00075-2, 1999.



- 684 Key, C. H. and Benson, N. C.: Landscape assessment: Sampling and analysis methods,
685 USDA For. Serv. Gen. Tech. Rep. RMRS-GTR-164-CD, (June), 1–55,
686 doi:10.1002/app.1994.070541203, 2006.
- 687 Klimont, Z., Kupiainen, K., Heyes, C., Purohit, P., Cofala, J., Rafaj, P., Borken-Kleefeld, J. and
688 Schöpp, W.: Global anthropogenic emissions of particulate matter including black
689 carbon, Atmos. Chem. Phys., 17, 8681–8723, doi:10.5194/acp-17-508681-2017, 2017.
- 690 Lavoie, C. and Pellerin, S.: Fires in temperate peatlands (southern Quebec): past and
691 recent trends, Can. J. Bot., 85(3), 263–272, doi:10.1139/B07-012, 2007.
- 692 Lelieveld, J., Evans, J. S., Fnais, M., Giannadaki, D. and Pozzer, A.: The contribution of
693 outdoor air pollution sources to premature mortality on a global scale., Nature,
694 525(7569), 367–71, doi:10.1038/nature15371, 2015.
- 695 Leung, F. Y. T., Logan, J. A., Park, R., Hyer, E., Kasischke, E., Streets, D. and Yurganov, L.:
696 Impacts of enhanced biomass burning in the boreal forests in 1998 on tropospheric
697 chemistry and the sensitivity of model results to the injection height of emissions, J.
698 Geophys. Res. Atmos., 112(10), 1–15, doi:10.1029/2006JD008132, 2007.
- 699 Magnan, G., Lavoie, M. and Payette, S.: Impact of fire on long-term vegetation dynamics
700 of ombrotrophic peatlands in northwestern Québec, Canada, Quat. Res., 77(1), 110–121,
701 doi:http://dx.doi.org/10.1016/j.yqres.2011.10.006, 2012.
- 702 Massling, A., Nielsen, I. E., Kristensen, D., Christensen, J. H., Sorensen, L. L., Jensen, B.,
703 Nguyen, Q. T., Nøjgaard, J. K., Glasius, M. and Skov, H.: Atmospheric black carbon and
704 sulfate concentrations in Northeast Greenland, Atmos. Chem. Phys., 15(16), 9681–9692,
705 doi:10.5194/acp-15-9681-2015, 2015.
- 706 Mayer, B. and Kylling, A.: Technical note: The libRadtran software package for radiative
707 transfer calculations - description and examples of use, Atmos. Chem. Phys., 5(7), 1855–
708 1877, doi:10.5194/acp-5-1855-2005, 2005.
- 709 Myhre, G., Shindell, D., Bréon, F.-M., Collins, W., Fuglestedt, J., Huang, J., Koch, D.,
710 Lamarque, J.-F., Lee, D., Mendoza, B., Nakajima, T., Robock, A., Stephens, G., Takemura, T.
711 and Zhang, H.: Anthropogenic and Natural Radiative Forcing, in Climate Change 2013:
712 The Physical Science Basis. Contribution of Working Group I to the Fifth Assessment
713 Report of the Intergovernmental Panel on Climate Change, edited by Stocker, T.F., D. Qin,
714 G.-K. Plattner, M. Tignor, S. K. Allen, J. Boschung, A. Nauels, Y. Xia, V. Bex, and P. M.
715 Midgley, pp. 659–740, Cambridge University Press, Cambridge, United Kingdom and
716 New York, NY, USA., 2013.
- 717 NASA: FIRMS. Web Fire Mapper, [online] Available from:
718 <https://firms.modaps.eosdis.nasa.gov/firemap/> (Accessed 5 September 2017a), 2017.
- 719 NASA: Roundtable: The Greenland Wildfire, [online] Available from:
720 <https://earthobservatory.nasa.gov/blogs/earthmatters/2017/08/10/roundtable-the-greenland-wildfire/> (Accessed 6 September 2017b), 2017.
- 721 NASA: Wildfires Continue to Beleaguer Western Canada, [online] Available from:
722 <https://www.nasa.gov/image-feature/goddard/2017/wildfires-continue-to-beleaguer-western-canada> (Accessed 29 October 2017c), 2017.
- 723 New Scientist Magazine: Largest ever wildfire in Greenland seen burning from space,
724 [online] Available from: <https://www.newscientist.com/article/2143159-largest-ever-wildfire-in-greenland-seen-burning-from-space/> (Accessed 6 September 2017), 2017.
- 725 Page, S. E., Siegert, F., Rieley, J. O., Boehm, H.-D. V., Jada, A. and Limin, S.: The amount of
726 carbon released from peat and forest fires in Indonesia during 1997, Nature, 420(19),
727 61–65, doi:10.1038/nature01131, 2015.
- 728 Paugam, R., Wooster, M. and Atherton, J.: Development and optimization of a wildfire
729 plume rise model based on remote sensing data inputs – Part 2, , doi:10.5194/acpd-15-



- 733 9815-2015, 2015.
- 734 Randerson, J. T., Chen, Y., Van Der Werf, G. R., Rogers, B. M. and Morton, D. C.: Global
735 burned area and biomass burning emissions from small fires, *J. Geophys. Res.*
736 *Biogeosciences*, 117(4), doi:10.1029/2012JG002128, 2012.
- 737 Reddy, A. D., Hawbaker, T. J., Wurster, F., Zhu, Z., Ward, S., Newcomb, D. and Murray, R.:
738 Quantifying soil carbon loss and uncertainty from a peatland wildfire using multi-
739 temporal LiDAR, *Remote Sens. Environ.*, 170, 306–316, doi:10.1016/j.rse.2015.09.017,
740 2015.
- 741 Rémy, S., Veira, A., Paugam, R., Sofiev, M., Kaiser, J. W., Marenco, F., Burton, S. P.,
742 Benedetti, A., Engelen, R. J., Ferrare, R. and Hair, J. W.: Two global data sets of daily fire
743 emission injection heights since 2003, , 2921–2942, doi:10.5194/acp-17-2921-2017,
744 2017.
- 745 Restuccia, F., Ptak, N. and Rein, G.: Self-heating behavior and ignition of shale rock,
746 *Combust. Flame*, 176, 213–219, doi:10.1016/j.combustflame.2016.09.025, 2017a.
- 747 Restuccia, F., Huang, X. and Rein, G.: Self-ignition of natural fuels: Can wildfires of
748 carbon-rich soil start by self-heating?, *Fire Saf. J.*, 91(February), 828–834,
749 doi:10.1016/j.firesaf.2017.03.052, 2017b.
- 750 Sand, M., Berntsen, T. K., von Salzen, K., Flanner, M. G., Langner, J. and Victor, D. G.:
751 Response of Arctic temperature to changes in emissions of short-lived climate forcers,
752 *Nat. Clim. Chang.*, 6(November), 1–5, doi:10.1038/nclimate2880, 2015.
- 753 von Schneidmesser, E., Schauer, J. J., Hagler, G. S. W. and Bergin, M. H.: Concentrations
754 and sources of carbonaceous aerosol in the atmosphere of Summit, Greenland, *Atmos.*
755 *Environ.*, 43(27), 4155–4162, doi:10.1016/j.atmosenv.2009.05.043, 2009.
- 756 Seiler, W. and Crutzen, P. J.: Estimates of gross and net fluxes of carbon between the
757 biosphere and the atmosphere from biomass burning, *Clim. Change*, 2(3), 207–247,
758 doi:10.1007/BF00137988, 1980.
- 759 SERMITSIAQ: Se billeder: Naturbrand udvikler kraftig røg, , in Danish [online] Available
760 from: <http://sermitsiaq.ag/se-billeder-naturbrand-udvikler-kraftig-roeg> (Accessed 6
761 September 2017), 2017.
- 762 Shetler, G., Turetsky, M. R., Kane, E. and Kasischke, E.: Sphagnum mosses limit total
763 carbon consumption during fire in Alaskan black spruce forests, *Can. J. For. Res.*, 38(8),
764 2328–2336, doi:10.1139/X08-057, 2008.
- 765 Shi, Y., Matsunaga, T., Saito, M., Yamaguchi, Y. and Chen, X.: Comparison of global
766 inventories of CO₂ emissions from biomass burning during 2002-2011 derived from
767 multiple satellite products, *Environ. Pollut.*, 206, 479–487,
768 doi:10.1016/j.envpol.2015.08.009, 2015.
- 769 Skeie, R. B., Berntsen, T., Myhre, G., Pedersen, C. A., Ström, J., Gerland, S. and Ogren, J. A.:
770 Black carbon in the atmosphere and snow, from pre-industrial times until present,
771 *Atmos. Chem. Phys.*, 11(14), 6809–6836, doi:10.5194/acp-11-6809-2011, 2011.
- 772 Smirnov, N. S., Korotkov, V. N. and Romanovskaya, A. A.: Black carbon emissions from
773 wildfires on forest lands of the Russian Federation in 2007–2012, *Russ. Meteorol.*
774 *Hydrol.*, 40(7), 435–442, doi:10.3103/S1068373915070018, 2015.
- 775 Stamnes, K., Tsay, S.-C., Wiscombe, W. and Jayaweera, K.: Numerically stable algorithm
776 for discrete-ordinate-method radiative transfer in multiple scattering and emitting
777 layered media, *Appl. Opt.*, 27(12), 2502, doi:10.1364/AO.27.002502, 1988.
- 778 Stendel, M., Christensen, J. H. and Petersen, D.: Arctic Climate and Climate Change with a
779 Focus on Greenland, *Adv. Ecol. Res.*, 40(7), 13–43, doi:10.1016/S0065-2504(07)00002-
780 5, 2008.
- 781 Stockwell, C. E., Jayarathne, T., Cochrane, M. A., Ryan, K. C., Putra, E. I., Saharjo, B. H.,



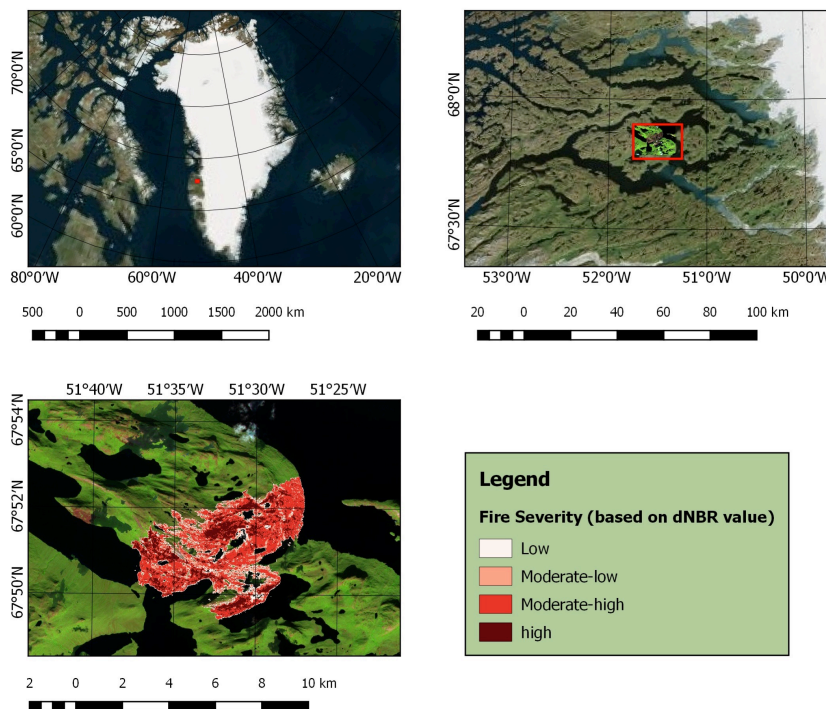
- 782 Nurhayati, A. D., Albar, I., Blake, D. R., Simpson, I. J., Stone, E. A. and Yokelson, R. J.: Field
783 measurements of trace gases and aerosols emitted by peat fires in Central Kalimantan,
784 Indonesia, during the 2015 El Niño, *Atmos. Chem. Phys.*, 16(18), 11711–11732,
785 doi:10.5194/acp-16-11711-2016, 2016.
- 786 Stohl, A., Forster, C., Frank, A., Seibert, P. and Wotawa, G.: Technical note: The Lagrangian
787 particle dispersion model FLEXPART version 6.2, *Atmos. Chem. Phys.*, 5(9), 2461–2474,
788 doi:10.5194/acp-5-2461-2005, 2005.
- 789 Stohl, A., Andrews, E., Burkhardt, J. F., Forster, C., Herber, A., Hoch, S. W., Kowal, D.,
790 Lunder, C., Mefford, T., Ogren, J. A., Sharma, S., Spichtinger, N., Stebel, K., Stone, R., Ström,
791 J., Tørseth, K., Wehrli, C. and Yttri, K. E.: Pan-Arctic enhancements of light absorbing
792 aerosol concentrations due to North American boreal forest fires during summer 2004, *J.*
793 *Geophys. Res. Atmos.*, 111(22), 1–20, doi:10.1029/2006JD007216, 2006.
- 794 Stohl, A., Berg, T., Burkhardt, J. F., Fjæraa, A. M., Forster, C., Herber, A., Hov, Ø., Lunder, C.,
795 McMillan, W. W., Oltmans, S., Shiobara, M., Simpson, D., Solberg, S., Stebel, K., Ström, J.,
796 Tørseth, K., Treffeisen, R., Virkkunen, K. and Yttri, K. E.: Arctic smoke – record
797 high air pollution levels in the European Arctic due to agricultural fires in Eastern
798 Europe in spring 2006, *Atmos. Chem. Phys.*, 7(2), 511–534, doi:10.5194/acp-7-511-
799 2007, 2007.
- 800 Stohl, A., Prata, A. J., Eckhardt, S., Clarisse, L., Durant, A., Henne, S., Kristiansen, N. I.,
801 Minikin, A., Schumann, U., Seibert, P., Stebel, K., Thomas, H. E., Thorsteinsson, T., Tørseth,
802 K. and Weinzierl, B.: Determination of time-and height-resolved volcanic ash emissions
803 and their use for quantitative ash dispersion modeling: The 2010 Eyjafjallajökull
804 eruption, *Atmos. Chem. Phys.*, 11(9), 4333–4351, doi:10.5194/acp-11-4333-2011, 2011.
- 805 Stohl, A., Klimont, Z., Eckhardt, S., Kupiainen, K., Shevchenko, V. P., Kopeikin, V. M. and
806 Novigatsky, A. N.: Black carbon in the Arctic: The underestimated role of gas flaring and
807 residential combustion emissions, *Atmos. Chem. Phys.*, 13(17), 8833–8855,
808 doi:10.5194/acp-13-8833-2013, 2013.
- 809 Stroeve, J., Box, J. E., Gao, F., Liang, S., Nolin, A. and Schaaf, C.: Accuracy assessment of the
810 MODIS 16-day albedo product for snow: Comparisons with Greenland in situ
811 measurements, *Remote Sens. Environ.*, 94(1), 46–60, doi:10.1016/j.rse.2004.09.001,
812 2005.
- 813 Sunderman, S. O. and Weisberg, P. J.: Remote sensing approaches for reconstructing fire
814 perimeters and burn severity mosaics in desert spring ecosystems, *Remote Sens.*
815 *Environ.*, 115(9), 2384–2389, doi:10.1016/j.rse.2011.05.001, 2011.
- 816 Turetsky, M. R., Donahue, W. F. and Benscoter, B. W.: Experimental drying intensifies
817 burning and carbon losses in a northern peatland, *Nat. Commun.*, 2, 514,
818 doi:10.1038/ncomms1523, 2011.
- 819 Turetsky, M. R., Benscoter, B., Page, S., Rein, G., van der Werf, G. R. and Watts, A.: Global
820 vulnerability of peatlands to fire and carbon loss, *Nat. Geosci.*, 8(1), 11–14,
821 doi:10.1038/ngeo2325, 2014.
- 822 Urbanski, S. P., Hao, W. M. and Nordgren, B.: The wildland fire emission inventory:
823 Western United States emission estimates and an evaluation of uncertainty, *Atmos.*
824 *Chem. Phys.*, 11(24), 12973–13000, doi:10.5194/acp-11-12973-2011, 2011.
- 825 Wandji Nyamsi, W., Arola, A., Blanc, P., Lindfors, a. V., Cesnulyte, V., Pitkänen, M. R. a. and
826 Wald, L.: Technical Note: A novel parameterization of the transmissivity due to ozone
827 absorption in the distribution method and correlated approximation of Kato et al.
828 (1999) over the UV band, *Atmos. Chem. Phys.*, 15(13), 7449–7456, doi:10.5194/acp-15-
829 7449-2015, 2015.
- 830 Warren, S. G.: Can black carbon in snow be detected by remote sensing?, *J. Geophys. Res.*



- 831 Atmos., 118(2), 779–786, doi:10.1029/2012JD018476, 2013.
- 832 Wieder, R. K., Scott, K. D., Kamminga, K., Vile, M. A., Vitt, D. H., Bone, T., Xu, B., Benscoter,
833 B. W. and Bhatti, J. S.: Postfire carbon balance in boreal bogs of Alberta, Canada, Glob.
834 Chang. Biol., 15(1), 63–81, doi:10.1111/j.1365-2486.2008.01756.x, 2009.
- 835 Winiger, P., Andersson, A., Eckhardt, S., Stohl, A., Semiletov, I. P., Dudarev, O. V., Charkin,
836 A., Shakhova, N., Klimont, Z., Heyes, C. and Gustafsson, Ö.: Siberian Arctic black carbon
837 sources constrained by model and observation, Proc. Natl. Acad. Sci., 114(7), E1054–
838 E1061, doi:10.1073/pnas.1613401114, 2017.
- 839 Winker, D. M., Vaughan, M. A., Omar, A., Hu, Y., Powell, K. A., Liu, Z., Hunt, W. H. and
840 Young, S. A.: Overview of the CALIPSO mission and CALIOP data processing algorithms, J.
841 Atmos. Ocean. Technol., 26(11), 2310–2323, doi:10.1175/2009JTECHA1281.1, 2009.
- 842 Wu, D., Huang, X., Norman, F., Verplaetsen, F., Berghmans, J. and Van Den Bulck, E.:
843 Experimental investigation on the self-ignition behaviour of coal dust accumulations in
844 oxy-fuel combustion system, Fuel, 160, 245–254, doi:10.1016/j.fuel.2015.07.050, 2015.
- 845
- 846

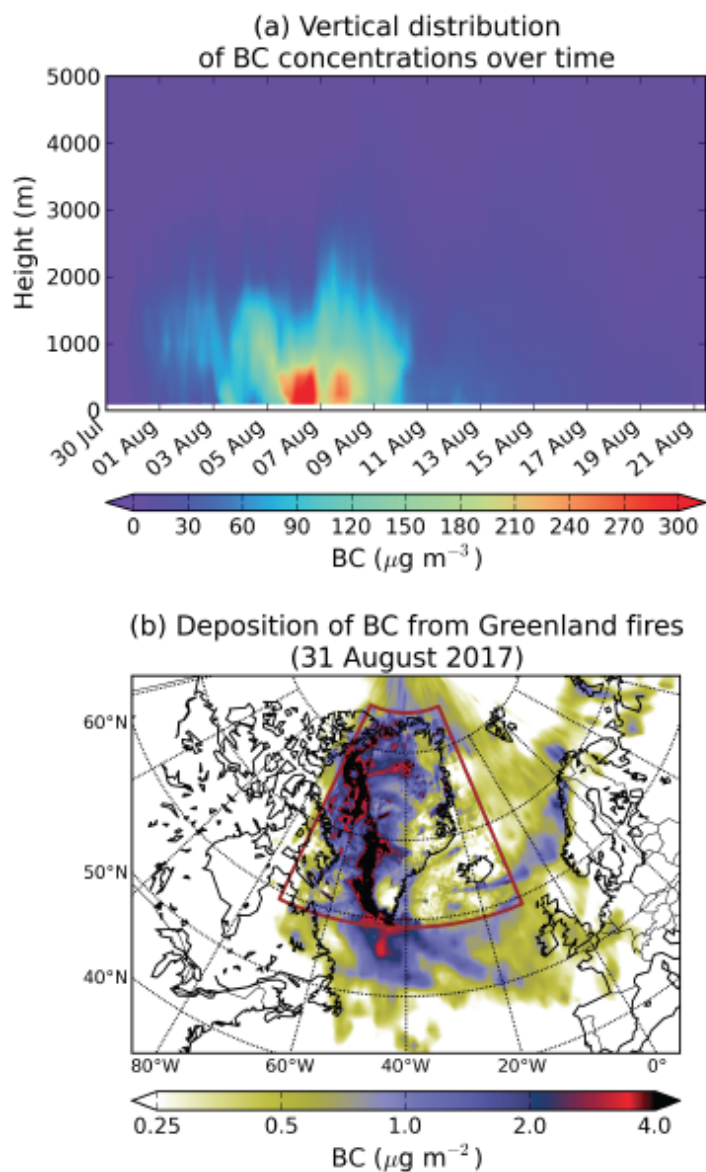


847 **FIGURE LEGENDS**



848
849 **Figure 1.** Map of Greenland (upper left) and zoomed map marked with fire location (upper
850 right and burned area classification (bottom) in terms of fire severity according to Sentinel 2A
851 images for fires burning in Greenland in August 2017. To delineate fire perimeters, both
852 Landsat 8 OLI and Sentinel 1A – 2A data were used (**Table 1**).

853



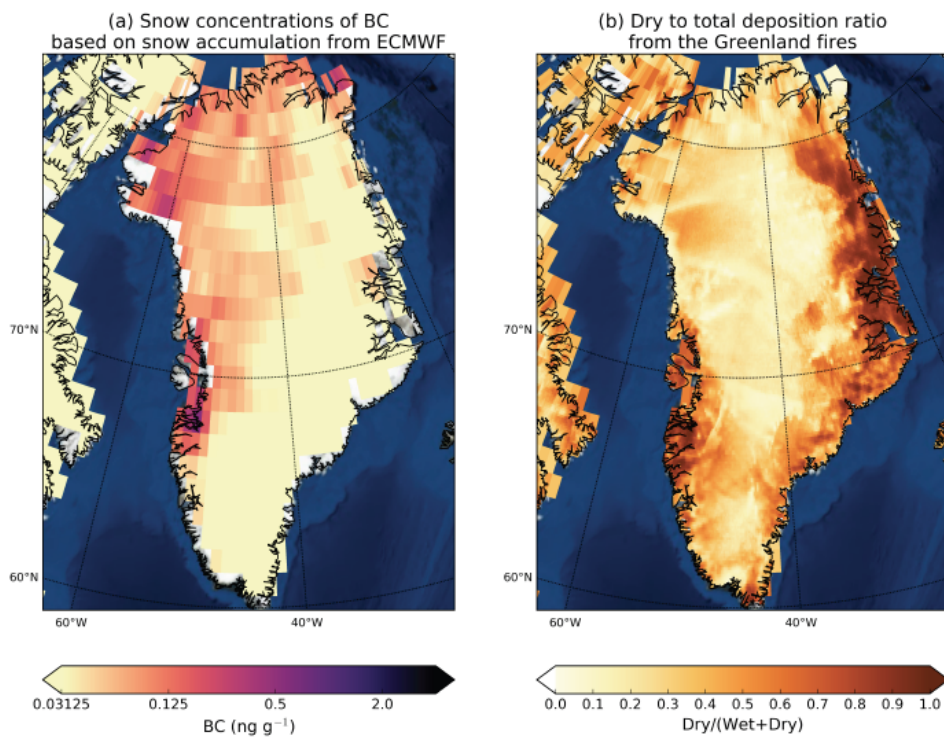
854

855 **Figure 2.** (a) Vertical distribution of BC concentrations from the fires in Greenland in
856 summer 2017 as a function of time. (b) Total (wet and dry) deposition of BC (in ng m^{-2}) from
857 Greenland fires until 31 August 2017. The colored rectangle depicts the nested high-
858 resolution domain.

859



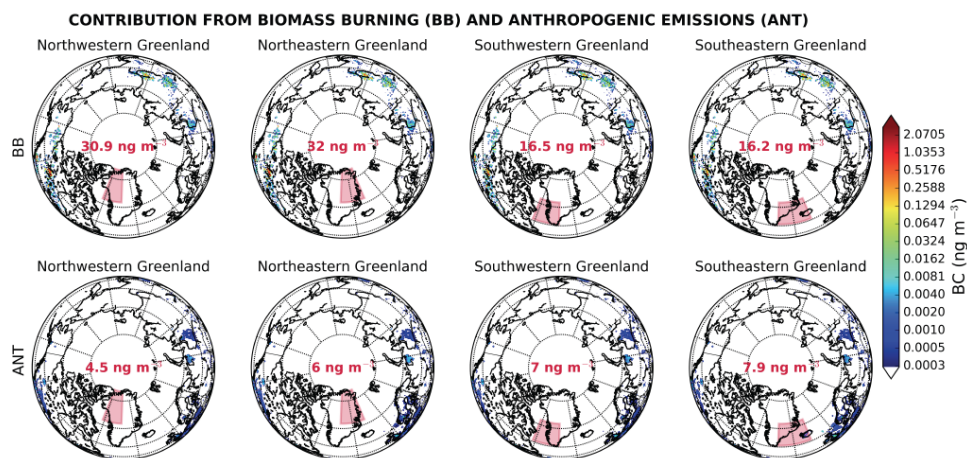
860



861

862 **Figure 3.** (a) Calculated snow concentrations of BC over Greenland based on the modeled
863 deposition and the snow precipitation (large scale and convective) in the operational ECMWF
864 data that were used in our simulation (see section 2.3). (b) Dry to total deposition ratio of BC
865 from the 2017 peat fires over Greenland.

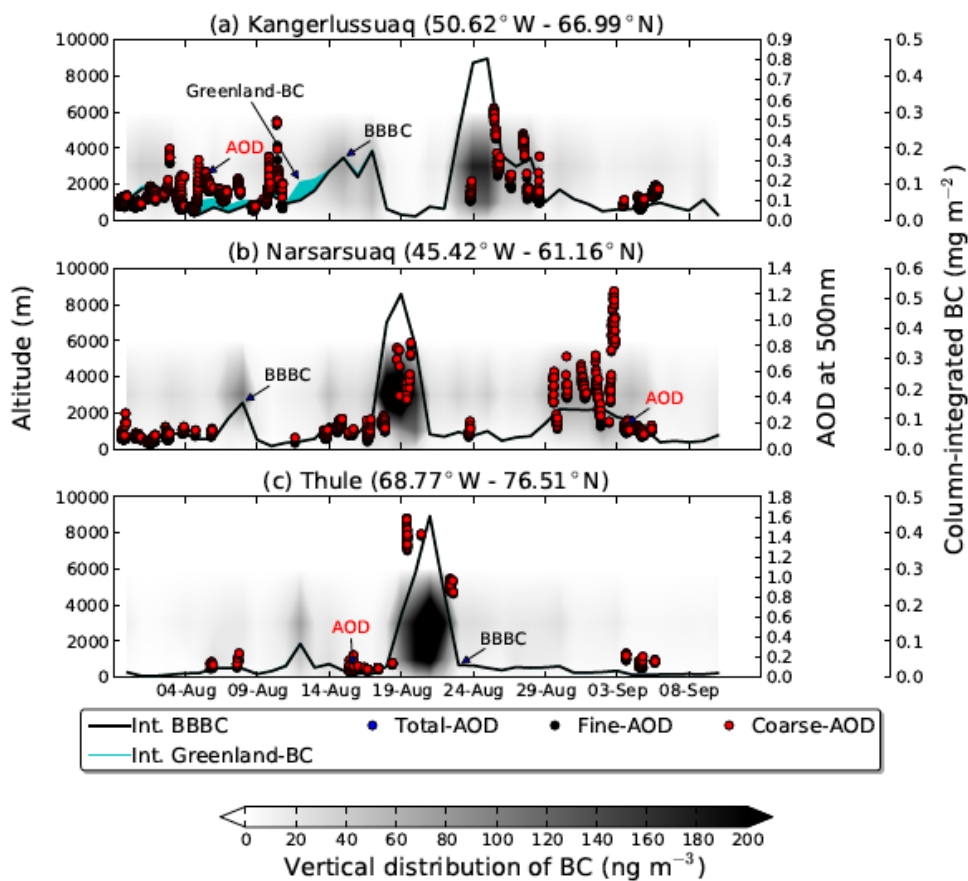
866



867

868 **Figure 4.** Average contribution of biomass burning (upper panels) and anthropogenic
869 emissions (lower panels) to surface concentrations of BC in Northwestern, Northeastern,
870 Southwestern and Southeastern Greenland (in ng m⁻³ per grid cell). Numbers (in red)
871 represent total concentrations in the studied domain, obtained by spatial integration over all
872 receptor areas in Greenland are highlighted by pink boxes.

873



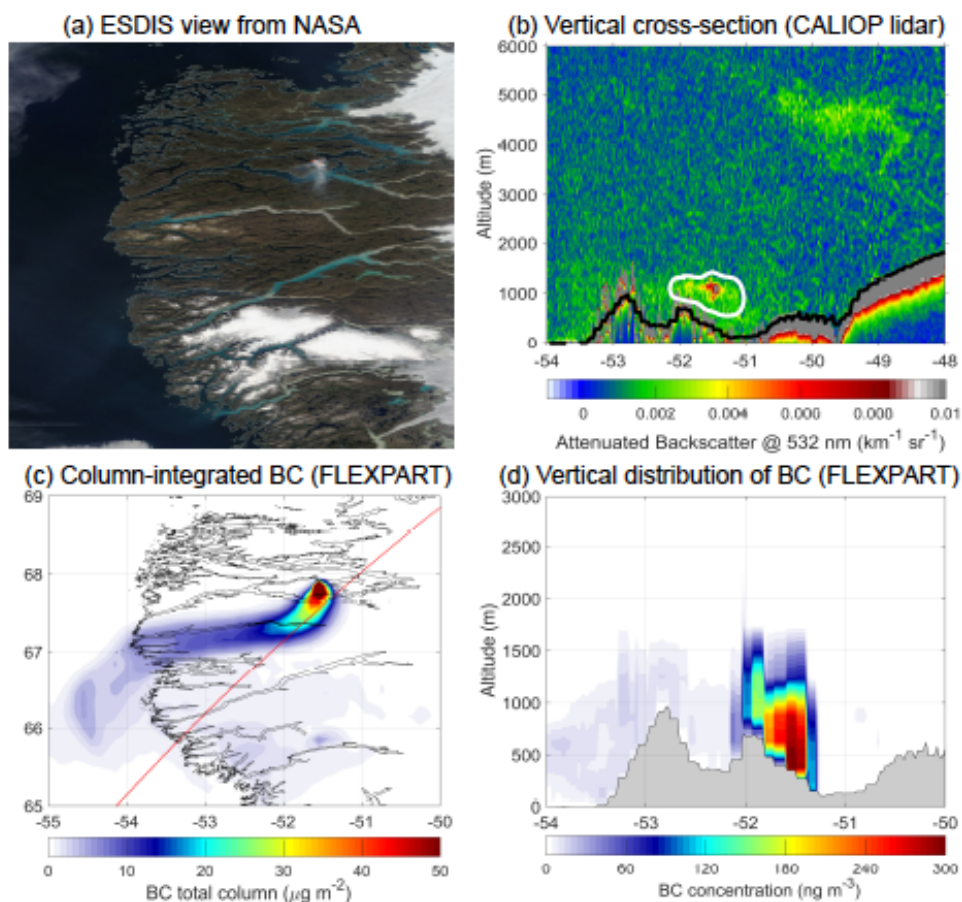
874

875 **Figure 5.** Contour plot of the vertical distribution of simulated BC (altitude shown on left y-
876 axis) as a function of time (x-axis) and time-series of column-integrated simulated BC
877 (extended right axis) from fires burning outside Greenland (black line) and Greenland fires
878 (cyan stacked area). Also shown are time-series of AOD measurements for fine (black),
879 coarse (red) and all (blue) aerosol particles at 500 nm (right y-axis). The three panels show
880 results for stations (a) Kangerlussuaq, (b) Narsarsuaq and (c) Thule (sorted from the closest to
881 the farthest station).

882



883



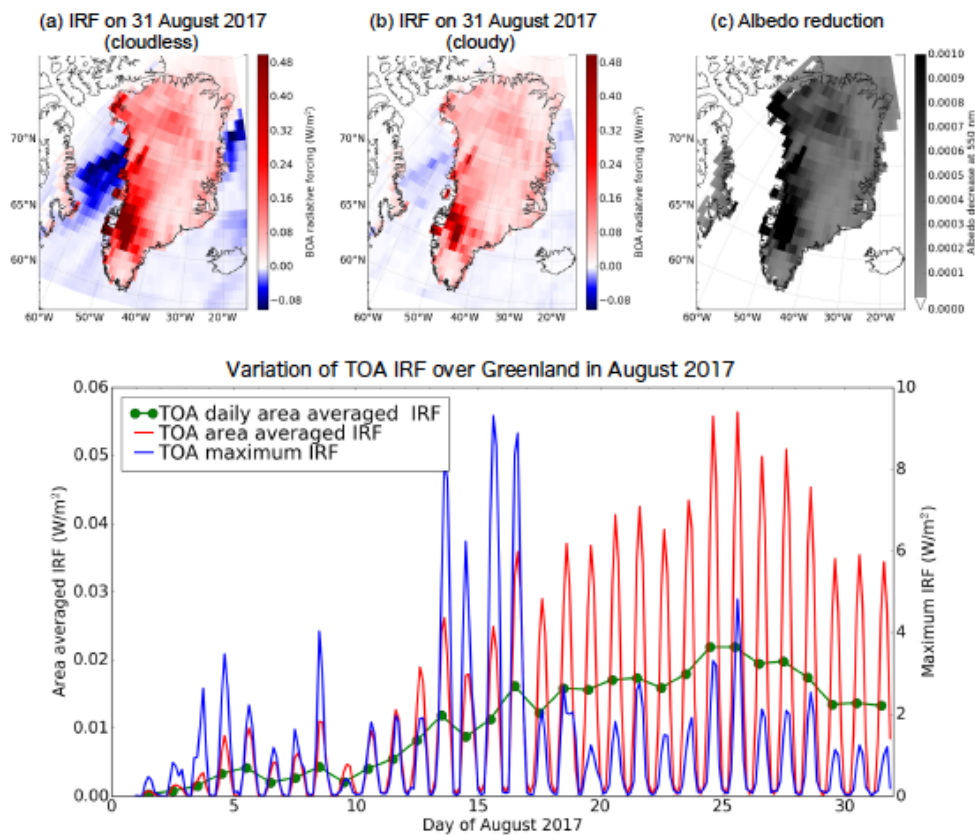
884

885 **Figure 6.** (a) Worldview application from the NASA/Goddard Space Flight Center Earth
886 Science Data and Information System (ESDIS) project on 14 August 2017. (b) Vertical cross-
887 section along satellite's route (red line in c) of total attenuated backscatter at a wavelength of
888 532 nm obtained from the CALIOP lidar on 14 August 2017 at 6 UTC (black line denotes the
889 orography of the area). (c) Column-integrated BC concentration simulated with FLEXPART
890 (red line shows the path of the satellite). (d) Vertical distribution of BC concentrations with
891 longitude as seen with FLEXPART (grey area denotes the orography of the area).

892



893



894

895 **Figure 7.** (a) The instantaneous direct BOA RF due to BC from the Greenland fires for
896 cloudless and (b) cloudy conditions on 31 August, and (c) the snow albedo reduction. (d)
897 Temporal variation of the TOA IRF over Greenland in August 2017.

898



Table 1. Start and end date of releases, source of data, type of sensor, burned area and daily increment of burned area, fuel consumption and calculated BC emissions from Eq. 1 during the Greenland fires in 2017. Total numbers for burned area, fuel consumption and BC emissions are highlighted in bold.

Start	End	Source of RS data	Type of sensor	Burned area (ha)	Increment of burned area (ha)	Fuel consumption (t C)	BC emission (kg)
31/07/17	02/08/17	Sentinel 2A	MSI	304	304	15176	3035
02/08/17	03/08/17	Landsat 8 OLI	MSI	428	125	6247	1249
03/08/17	04/08/17	Sentinel 1A	SAR	588	160	7980	1596
04/08/17	05/08/17	Sentinel 1A	SAR	740	152	7621	1524
05/08/17	07/08/17	Sentinel 2A	MSI	1100	359	17966	3593
07/08/17	08/08/17	Sentinel 2A	MSI	1314	214	10706	2141
08/08/17	12/08/17	Landsat 8 OLI	MSI	1868	554	27714	5543
12/08/17	14/08/17	Sentinel 1A	SAR	2005	136	6817	1363
14/08/17	15/08/17	Sentinel 1A	SAR	2169	165	8244	1649
15/08/17	16/08/17	Sentinel 1A	SAR	2209	40	1998	400
16/08/17	19/08/17	Sentinel 1A	SAR	2254	44	2213	443
19/08/17	21/08/17	Sentinel 2A	MSI	2345	92	4579	916
TOTAL					2345	117259	23452

RS - Remote Sensing
 MSI - Multispectral Images
 SAR - Synthetic Aperture RADAR